



Interannual variability of Kelvin wave propagation in the wave guides of the equatorial Indian Ocean, the coastal Bay of Bengal and the southeastern Arabian Sea during 1993–2006

R.R. Rao^a, M.S. Girish Kumar^b, M. Ravichandran^{b,*}, A.R. Rao^c, V.V. Gopalakrishna^d, P. Thadathil^e

^a Japan Marine Earth Science and Technology, Yokosuka 237 0061, Japan

^b Indian National Centre for Ocean Information Services, Hyderabad 500 055, India

^c Naval Physical and Oceanographic Laboratory, Kochi 682 021, India

^d National Institute of Oceanography, Goa 403 004, India

^e Embassy of India, Tokyo 102 0074, Japan

ARTICLE INFO

Article history:

Received 15 December 2008

Received in revised form

5 October 2009

Accepted 9 October 2009

Available online 31 October 2009

ABSTRACT

The observed variability of the Kelvin waves and their propagation in the equatorial wave guide of the Indian Ocean and in the coastal wave guides of the Bay of Bengal (BoB) and the southeastern Arabian Sea (AS) on seasonal to interannual time scales during years 1993–2006 is examined utilizing all the available satellite and in-situ measurements. The Kelvin wave regime inferred from the satellite-derived sea surface height anomalies (SSHA) shows a distinct annual cycle composed of two pairs of alternate upwelling (first one occurring during January–March and the second one occurring during August–September) and downwelling (first one occurring during April–June and the second one occurring during October–December) Kelvin waves that propagate eastward along the equator and hit the Sumatra coast and bifurcate. The northern branches propagate counterclockwise over varied distances along the coastal wave guide of the BoB. The potential mechanisms that contribute to the mid-way termination of the first upwelling and the first downwelling Kelvin waves in the wave guide of the BoB are hypothesized. The second downwelling Kelvin wave alone reaches the southeastern AS, and it shows large interannual variability caused primarily by similar variability in the equatorial westerly winds during boreal fall. The westward propagating downwelling Rossby waves triggered by the second downwelling Kelvin wave off the eastern rim of the BoB also shows large interannual variability in the near surface thermal structure derived from SODA analysis. The strength of the equatorial westerlies driven by the east–west gradient of the heat sources in the troposphere appears to be a critical factor in determining the observed interannual variability of the second downwelling Kelvin wave in the wave guides of the equatorial Indian Ocean, the coastal BoB, and the southeastern AS.

© 2009 Elsevier Ltd. All rights reserved.

1. Introduction

The observed near-surface circulation in the equatorial Indian Ocean (EIO), the Arabian Sea (AS) and the Bay of Bengal (BoB) manifests itself primarily through Ekman and geostrophic adjustments and responds rapidly to the seasonal changes in the monsoonal surface wind and buoyancy forcings (Duing, 1970; Wyrtki, 1973; Cutler and Swallow, 1984; Luther and O'Brien, 1985; Reverdin, 1987; Woodbury et al., 1989; Molinari et al., 1990; Hastenrath and Greischar, 1991; Schiller et al., 1998; Shetye and Gouveia, 1998; Shenoi et al., 1999; Schott and McCreary, 2001; Shankar et al., 2002; Somayajulu et al., 2003;

Sengupta et al., 2004; Masumoto et al., 2005, 2008; Schott et al., 2009; Hase et al., 2008; Nagura and McPhaden, 2008; Ogata et al., 2008; Horii et al., 2008; Iskandar et al., 2009). In addition, the planetary scale waves – Rossby, Yanai, equatorial and coastal Kelvin waves driven by the surface wind and buoyancy flux fields – also influence the near-surface circulation of these basins through both local and remote effects (Lighthill, 1969; Cane, 1980; Gent et al., 1983; Kindle and Thompson, 1989; Moore and McCreary, 1990; Potemra et al., 1991; Yu et al., 1991; Tsai et al., 1992; Perigaud and Delecluse, 1992, 1993; McCreary et al., 1993, 1996; Bruce et al., 1994, 1998; Prasannakumar and Unnikrishnan, 1995; Yamagata et al., 1996; Vinayachandran et al., 1996; Shankar and Shetye, 1997; Vinayachandran and Yamagata, 1998; Chambers et al., 1999; Murtugudde and Busalacchi, 1999; White, 2000; Eigenheer and Quadfasel, 2000; Basu et al., 2000; Murtugudde et al., 2000; Sprintall et al., 2000; Gopalan et al., 2000; Le Blanc

* Corresponding author.

E-mail address: ravi@incois.gov.in (M. Ravichandran).

and Boulanger, 2001; Schott and McCreary, 2001; Shankar et al., 2002; Haugen et al., 2002; Han and Webster, 2002; Brandt et al., 2002; Yu, 2003; Han, 2005; Miyama et al., 2006; Yuan and Han, 2006; Schott et al., 2009). With the availability of high-resolution and accurate satellite altimetry measurements, considerable interest is evinced in the recent literature on the planetary scale wave propagation and its potential influence on basin-scale and coastal circulation regimes. The signature of the westward propagating Rossby waves as seen in altimetry measurements and in the numerical model simulations for the tropical Indian Ocean is very well documented in the literature. Polito and Liu (2003) have characterized the spectral nature of the Rossby waves in the global ocean. They have reported that the clearest and most energetic wave signals are generally observed for the annual and that the semiannual Rossby waves often have the largest amplitudes near the tropics. In the EIO, the zonal winds, semiannual in nature, remotely generate corresponding semiannual sea-level fluctuations near the eastern equator (Clark and Liu, 1993). The observed interannual sea-level signal along the eastern and northern Indian Ocean boundary is generated remotely by interannual equatorial zonal winds (Clark and Liu, 1994). Along the equatorial wave guide in the Indian Ocean, Yu et al. (1991) have shown that the eastward propagating annual Kelvin wave, on reflection from the eastern boundary, propagates along the coastal wave guide of the BoB as a coastal Kelvin wave, radiating westward propagating Rossby waves into the interior BoB and influencing the East India Coastal Current (EICC). McCreary et al. (1993) have further shown that the winds along the eastern rim of the BoB also trigger similar Kelvin waves, which not only influence the EICC, but also turn around Sri Lanka to propagate poleward along the west coast of India, influencing West India Coastal Current (WICC). The observed annual cycle of Lakshadweep High and Low in the geopotential topography (Wyrtki, 1971; Bruce et al., 1994; Peter and Mizuno, 2000) and satellite altimetry (Ali et al., 1998; Gopalan et al., 2000) is attributed to the Rossby wave radiation by these coastal Kelvin waves off the southwest coast of India (McCreary et al., 1993; Bruce et al., 1994; Shankar and Shetye, 1997; Shankar et al., 2002). Shankar et al. (2002) have carried out a detailed study highlighting the relative importance of both local and remote processes that modulate the sea level and circulation in the northern Indian Ocean. Their study has clearly revealed that the equatorial zonal winds and the alongshore winds off the Myanmar coast have a weaker role in modulating the upwelling and downwelling cycles observed along the southwest coast of India. Prasad and Ikeda (2001) have shown the westward propagation of both Arabian Sea High and Lakshadweep High during January–March as the manifestations of Rossby waves. Basu et al. (2000) have shown that the annual signal in the Indian Ocean north of 10°S is composed of propagating and non-propagating modes. Subrahmanyam et al. (2001) have shown that the downwelling Kelvin waves play an important role by way of reflected and radiated Rossby waves. They have also shown the propagation of poleward coastal Kelvin waves along the west coast of India and the associated radiation of Rossby waves. Han and Webster (2002) have shown that in the BoB, the SSH anomalies near the eastern and northern boundaries are predominantly caused by equatorial wind variability, which generates coastal Kelvin waves that propagate into the bay along the eastern boundary. Hareesh Kumar and Sanilkumar (2004) have reported dominant variability in the SSHA field with 30–40 days, 3–4, 6 and 12 month periods in the coastal regions of the northern Indian Ocean. In a 1.5-layer reduced gravity model simulation, Rahul et al. (2004) have shown the occurrence of westward propagating twin gyres on either side of the equator as the reflected Rossby waves during June–August and November–December in response to the impinging equatorial jets on the

coast of Sumatra. In the southern tropical Indian Ocean in the latitudinal band of $8^{\circ}\text{--}20^{\circ}\text{S}$, Masumoto and Meyers (1998) have shown the occurrence of westward propagating annual Rossby wave both in the XBT data and in a model simulation. Wang et al. (2001) have explained the mechanisms that cause the breakup in the westward propagation of the annual Rossby wave in the mid-ocean resulting in two local maxima. Thus, these modeling studies have shown that in the northern Indian Ocean the coastal Kelvin waves play an important role in the coupling of the EICC and the WICC and triggering westward propagating Rossby waves across the basin. However, the propagation of these boundary waves into the southeastern AS has not been confirmed by observations (Schott and McCreary, 2001). In this study, utilizing all the available satellite and in-situ measurements the following issues are addressed:

- Identification of pathways of two pairs of alternate upwelling and downwelling Kelvin waves in the wave guides of the EIO, the coastal BoB, and the southeastern AS and the possible reasons for their mid-way termination before reaching the southeastern AS with the lone exception of the second downwelling Kelvin wave.
- Observed interannual variability of the second downwelling Kelvin wave in the wave guides of the equator, the coastal BoB, and the southeastern AS and its possible mechanism.
- Observed interannual variability of the westward propagation of Rossby waves in the northern EIO.
- Potential mechanism of stronger equatorial westerlies (during boreal fall) when the second downwelling Kelvin wave and its interannual variability are more pronounced.

It would be interesting to see the propagation signatures of the Kelvin waves in the wave guides of the EIO, the coastal BoB, and the southeastern AS in the observations. The recently-blended high-resolution Topex–Poseidon satellite altimetry measurements provide a unique opportunity to identify and track the propagation of these Kelvin waves in the wave guides of the equator, the coastal BoB, and the southeastern AS. In Section 2, all the data sets utilized to address the above issues are described. In Section 3, the signatures of the Kelvin wave trajectories and the probable governing mechanisms that terminate the propagation of both the upwelling and first downwelling Kelvin waves are suggested. The observed interannual variability of the second downwelling Kelvin wave in the wave guides of the EIO, the coastal BoB, and the southeastern AS is examined. The potential influence of this interannual variability of these Kelvin waves on the westward propagation of Rossby waves in the northern EIO is examined. The potential mechanism of stronger equatorial westerlies observed during strong second downwelling Kelvin wave regime is examined.

2. Observations

Several types of archived historic satellite and in-situ measurements are assembled and exploited to describe and understand the observed variability of the Kelvin waves in the northern Indian Ocean. The AVISO merged and blended SSHA data are utilized to characterize the signature of the propagating Kelvin and Rossby waves. The QuikSCAT surface winds (Wentz et al., 2001) are utilized to assess their impact on the observed equatorial and coastal Kelvin waves. The depth of the 20°C isotherm (D20) derived from the near-surface temperature climatology of Locarnini et al. (2006) is utilized to characterize Kelvin wave propagation along the equator. The multi-year averages of TRMM TMI SST (Wentz et al., 2000) are utilized to

Table 1.

Parameter	Source	Period	Accuracy	Spatial resolution
ERS1/2 Winds	www.cersat.ifremer.fr	1993–1999	1 m/s and 14°	1.0°
QuikSCAT Winds	www.ssmi.com	2000–2006	2 m/s	0.25°
AVISO Blended SSHA	www.aviso.oceanobs.com	1993–2006	2.5–4 cm	0.33°
TMI SST	www.ssmi.com	1998–2006	~0.5 °C	0.25°
Depth of 20 °C isotherm	www.jamstec.go.jp	2001–2006	Unknown	–
Tide gauge sea level	www.pol.ac.uk	1993–2004	1.0 cm	–
Near-surface vertical thermal structure (SODA V1.4.2 for period 1993–2001 and V2.0.4 for period 2002–2006)	www.dsrs.atmos.umd.edu	1993–2005	~0.5 °C	–
Outgoing long wave radiation	www.cdc.noaa.gov/cdc/data.interp_OLR.html	1993–2006	10 W/m ²	2.5°

characterize the background SST at the head of the BoB during boreal winter when the clockwise eddy circulation is present. The D20 derived from the data collected by a JAMSTEC mooring at 1.5°S and 90°E is utilized to seek its relationship with the surface zonal wind speed in the central EIO. The tide gauge data collected at three representative coastal stations – Visakhapatnam, Chennai, and Cochin – are utilized to characterize the observed in-situ sea-level variability along the east and southwest coasts of India. The near-surface thermal structure derived from SODA analysis (Carton et al., 2000) is utilized to characterize the westward propagation of Rossby waves in the north EIO during the following six months (October–March) of the second downwelling Kelvin wave generation. The outgoing long-wave radiation data of NOAA are utilized as a proxy to atmospheric convection to explain the observed variability of the strong westerly winds over the equatorial region. The sources, periods, accuracies and resolutions of the data sets utilized in this study are shown in Table 1.

3. Analysis

3.1. Annual cycle of SSHA in the northern Indian Ocean

The satellite-altimeter-derived SSHA field characterizes dynamic topography that is related to circulation and density field of the entire water column. The SSHA field in the ocean contains information of both steric effects and the effects of stationary and propagating planetary scale waves (Fu, 2001). The monsoon driven northern Indian Ocean shows a distinct annual cycle in the multi-year averaged SSHA field (Subrahmanyam and Robinson, 2000) (Fig. 1a). During a year, in the EIO, two pairs of upwelling and downwelling Kelvin waves alternately propagate eastward. In response to this, the thermocline in the eastern EIO shows large-amplitude vertical excursions with semi-annual periodicity (Rao and Sivakumar, 2000; Hase et al., 2008). The eastern equatorial region shows the signatures of these upwelling (downwelling) Kelvin waves during January–March and August–September (April–June and October–December). Both these two pairs of Kelvin waves hit the Sumatra coast and bifurcate as northward and southward propagating coastally trapped waves (Iskandar et al., 2009). The northern branches propagate over varied distances along the coastal wave guide of the BoB. These Kelvin waves also trigger Rossby waves from the eastern rim of the BoB that propagate westward in the northern EIO and in the BoB (McCreary et al., 1993; Iskandar et al., 2009). The AS is characterized by the westward propagating downwelling (upwelling) Rossby waves triggered off the southwest coast of India and further reinforced by the local wind stress curl forcing during December–April (June–October). These downwelling

(upwelling) Rossby waves produce large positive (negative) anomalies in the SSHA field in the southwestern AS during March–April (December–January). The AS shows large variability in the SSHA field in response to the summer monsoonal wind forcing. The associated strong negative (positive) surface wind stress curl results in strong positive (negative) SSHA in the south-central (coastal) AS. In the southwestern BoB, strong negative (positive) SSHA occurs in response to strong positive (negative) surface wind stress curl during September–December (January–April). South of the equator, in the east, the signature of the westward propagating upwelling (downwelling) Rossby wave is clearly seen during February–May (August–December) (Reverdin and Luyten, 1986). The Fourier analysis of mean monthly SSHA clearly shows the geographic regions where the annual (CPY: 1) and semi-annual (CPY: 2) modes are most dominant (Fig. 1b). The annual mode shows largest amplitude with large percent variance off the southwest coast of India, in the southern AS, off the Arabia coast, off the southwestern rim of the BoB and south of the equator in the east due to westward Rossby wave propagation. The semi-annual mode shows largest amplitude off the Sumatra coast due to impinging Kelvin waves along the equator from the west and the radiated Rossby waves towards the west. The western EIO also shows large signals on either side of the equator caused by the westward-propagating Rossby waves (Peter and Mizuno, 2000; Rao and Sivakumar, 2000). The coastal wave guide of the BoB also shows large values due to propagating Kelvin wave activity on both annual and semi-annual modes.

3.2. Kelvin waves in the EIO

The recent modeling studies have clearly revealed that the surface winds over the EIO play an important role in modulating the circulation features of the northern Indian Ocean through remote effects (Potemra et al., 1991; Yu et al., 1991; McCreary et al., 1993, 1996; Shankar et al., 2002). Changes in thermocline depth can be directly driven by the local winds as well as by the remote effects through the propagating baroclinic waves in the ocean. When westerly (easterly) winds blow over the equator, downwelling- (upwelling-) favorable equatorially trapped Kelvin waves radiate into the eastern ocean, deepening (shoaling) the thermocline there. These waves reflect from the eastern boundary as packets of coastally trapped Kelvin and Rossby waves, spreading the deepening/shoaling well off the equator. Waves can also be generated in off-equatorial regions through forcing by a patch of anticyclonic (downwelling) Ekman pumping in the eastern ocean. Then downwelling-favorable Rossby waves radiate from the forcing region, deepening the thermocline in the western ocean (Schott et al., 2009). In the Indian Ocean, the energy imparted by the surface wind field is carried eastward along the

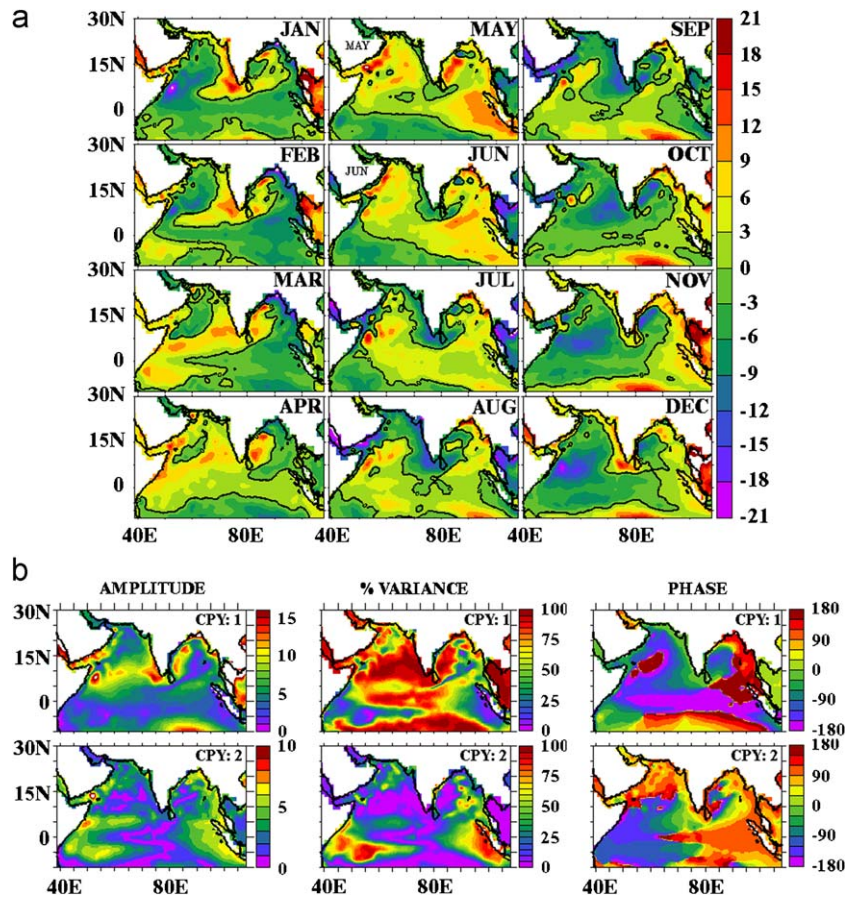


Fig. 1. (a) Observed annual cycle of multi-year (1993–2006) averaged SSHA in the north Indian Ocean. (b) Fourier fields of amplitude (cm), percent variance (%) and phase (deg) for CPY: 1 (upper panel) and CPY: 2 (lower panel) of SSHA in the north Indian Ocean.

equatorial wave guide as both downwelling and upwelling Kelvin waves and traverse around the rim of the BoB. In addition, the alongshore winds in the coastal BoB also trigger and modulate these propagating Kelvin waves. The signature of this wave propagation along the equator is examined with the satellite-derived altimetry and surface wind measurements. The observed climatology of the zonal wind stress (Fig. 2a) shows that the zonal winds are mostly westerly throughout the year with stronger magnitudes over the east-central equatorial region. Strong intraseasonal variability with pronounced peaks during the monsoon transitions is also noticed when spring and fall Wyrtki jets occur (Sengupta et al., 2001; Senan et al., 2003). These westerly wind bursts produce downwelling Kelvin waves that propagate eastward along the equator (O'Brien and Hurlburt, 1974; McPhaden, 1982; Visbeck and Schott, 1992; Jensen, 1993; Han et al., 1999, 2001; Miyama et al., 2006). When these westerly wind bursts weaken during July–August or are replaced by easterlies during boreal winter, the upwelling Kelvin waves are triggered and propagate eastward along the equator. In a year, two pairs of upwelling and downwelling Kelvin waves propagate alternately eastward. The signatures of these upwelling and downwelling Kelvin waves are also very well captured in the longitude-time fields of D20 extracted from the temperature climatology of Locarnini et al. (2006) (Fig. 2b) and SSHA climatology (Fig. 2c). Both these fields show a strong eastward propagating semi-annual signals along the equator. The deepening (shoaling) of D20 and increase (decrease) of SSHA during February–May (November–March) and August–November (May–September) is a clear manifestation of the downwelling (upwelling) Kelvin waves. In addition, these Kelvin waves also

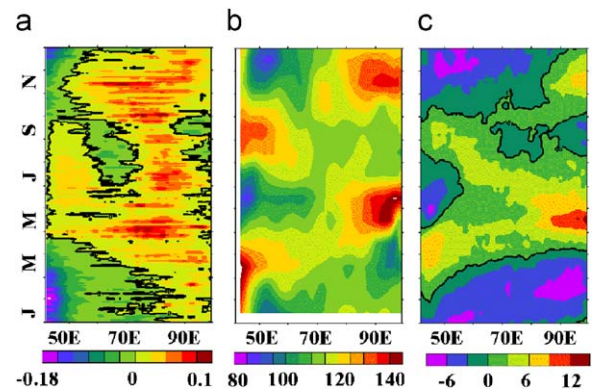


Fig. 2. Longitude-time sections of multi-year averages of (a) surface zonal wind stress (N/m^2), (b) D20 (m) and (c) SSHA (cm) along the equator (1°N – 1°S averages) in the Indian Ocean (zero contour is shown with thick black line).

reflect (trigger) Rossby waves that propagate westward both along and off the equator (Potemra et al., 1991; Yu et al., 1991).

3.3. Annual cycle of the Kelvin wave regime in the coastal wave guides of the BoB and the southeastern AS

The observed signatures of the Kelvin waves in the coastal wave guides of the BoB and the southeastern AS over a year are examined utilizing the SSHA climatology. Two pairs of the equatorial upwelling (downwelling) Kelvin waves show their counterclockwise propagation northward from the Sumatra coast

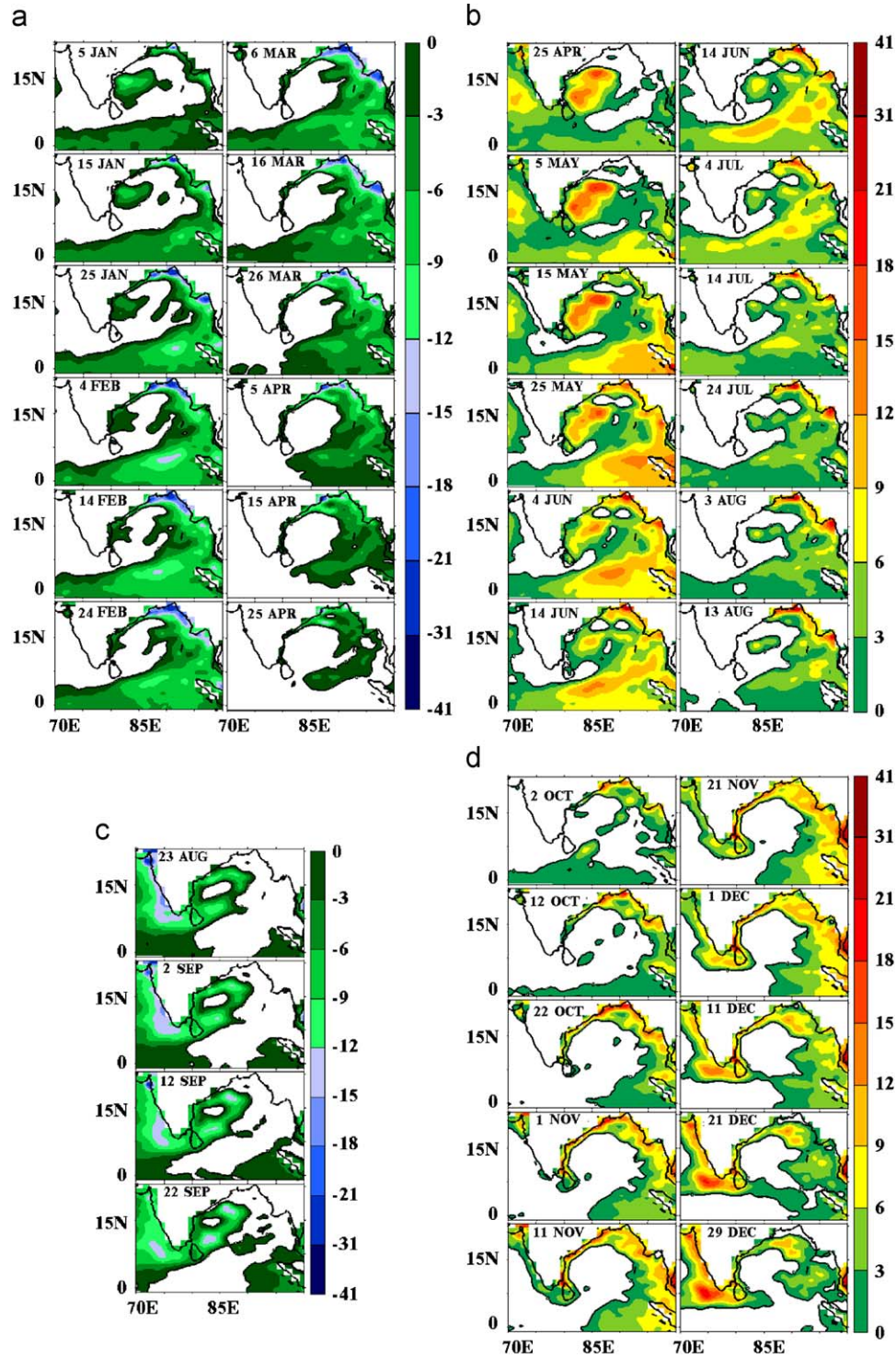


Fig. 3. (a) Evolution of the observed life cycle of the first upwelling Kelvin wave as seen from the multi-year averages of SSHA (cm) (only negative values are mapped) in the BoB at 10-day interval during 5 January–25 April. (b) Evolution of the observed life cycle of the first downwelling Kelvin wave as seen from the multi-year averages of SSHA (cm) (only positive values are mapped) in the BoB at 10-day interval during 25 April–13 August. (c) Evolution of the observed life cycle of the second upwelling Kelvin wave as seen from the multi-year averages of SSHA (cm) (only negative values are mapped) in the BoB at 10-day interval during 23 August–22 September. (d) Evolution of the observed life cycle of the second downwelling Kelvin wave as seen from the multi-year averages of SSHA (cm) (only positive values are mapped) in the BoB and the southeastern AS at 10 day interval during 2 October–29 December. (e) Schematic of the observed annual cycle of the propagating upwelling (blue wriggled arrows) and downwelling (red wriggled arrows) Kelvin waves along the wave guides of the equator, coastal BoB and coastal southeastern AS. (f) Longitude-time sections of observed multi-year averaged annual cycle of surface zonal wind speed (m/s) (left panel) and its interannual variance (m^2/s^2) (right panel) along the equator in the Indian Ocean. (g) Evolution of the clockwise eddy over the head of the BoB in the multi-year averaged near-surface circulation (Ekman+geostrophic) and the TMI SST ($^{\circ}\text{C}$) during December–March. (h) Evolution of the multi-year averaged East India Coastal Current (Ekman+geostrophic) off the east coast of India during April–June and October–December (arrow head shows the direction of the current and the arrow length and the background color show the current speed in cm/s) (for interpretation of the references to color in this figure legend, the reader is referred to the web version of this article).

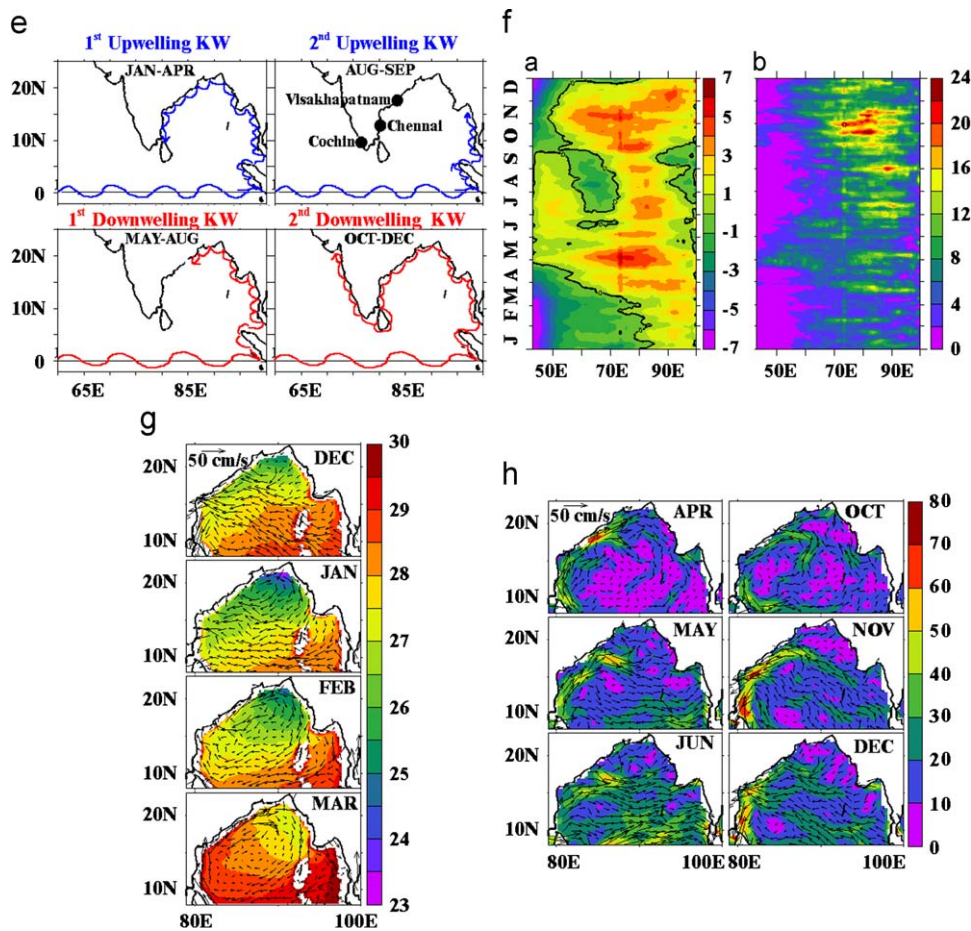


Fig. 3. (Continued)

over varied distances in the coastal wave guide of the BoB. In the BoB, the first upwelling (downwelling) Kelvin wave occurs during January–March (May–August) and the second upwelling (downwelling) Kelvin wave occurs during August–September (October–December) as shown in Fig. 3. All the four Kelvin waves show distinct life cycles geographically limited to the coastal wave guide of the BoB with only the exception of the second downwelling Kelvin wave. The first upwelling Kelvin wave while propagating along the wave guide radiates Rossby waves off the southeastern rim of the BoB. It attains its peak amplitude at the head of the bay during mid-February–mid-March. However, it weakens off the western rim of the BoB and terminates off the southeast coast of India (Fig. 3a). This suggests that this first upwelling Kelvin wave appears to have no significant role in remotely triggering coastal upwelling observed off the southwest coast of India as early as February/March. In tune with the modeling study of Shankar et al. (2002), the recent observational study of Gopalakrishna et al. (2008) has clearly revealed that the alongshore wind stress off the southwest coast of India and the remote forcing from south of Sri Lanka are more important forcings compared with the equatorial forcing influencing the upwelling signal in the Lakshadweep Sea during the summer monsoon season. The propagation of the first downwelling Kelvin wave also terminates mid-way in the coastal wave guide off the head of the BoB (Fig. 3b). Large positive values seen off the mouths of major rivers Ganges–Brahmaputra and Irrawaddy suggest the influence of fresh water flux on the observed SSHA. Among all the four Kelvin waves, the second upwelling Kelvin wave is the least developed and is only limited to southeastern rim of the BoB. Among both the pairs of upwelling and

downwelling Kelvin waves, only the second downwelling Kelvin wave is the most pronounced. Among all these four waves, this wave alone propagates all through the coastal wave guide of the BoB, turns around Sri Lanka, and then propagates along the west coast of India. The signatures of the propagation trajectories of both the upwelling and downwelling Kelvin waves along the equator and in the coastal wave guides of the BoB and the southeastern AS are schematically summarized in Fig. 3e.

It is important to understand the reasons for the mid-way termination of both the upwelling Kelvin waves and the first downwelling Kelvin wave before they reach the coastal southeastern AS. The probable mechanisms that govern the mid-way termination of both the upwelling Kelvin waves and the first downwelling Kelvin wave and the entry of the second downwelling Kelvin wave into the coastal southeastern AS are examined. A careful examination of the observed climatology of the annual cycle of the surface zonal winds along the equator shows an oscillatory nature on intraseasonal time scales (Fig. 3f). In general the westerly (easterly) winds occur over relatively longer (shorter) durations and are relatively stronger (weaker). During December–February along the equator the easterly winds are stronger than those during August–September, clearly explaining the difference in the pathways of the upwelling Kelvin waves in the coastal wave guide of the BoB (Fig. 3e). The patch of westerly winds is stronger and wider in spatio-temporal extent during the fall transition than during the spring transition (Fig. 3f). In view of this differential forcing, the first downwelling Kelvin wave terminates at the head of the bay while the second downwelling Kelvin wave enters the coastal southeastern AS. At the head of the BoB, during December–February, a clockwise

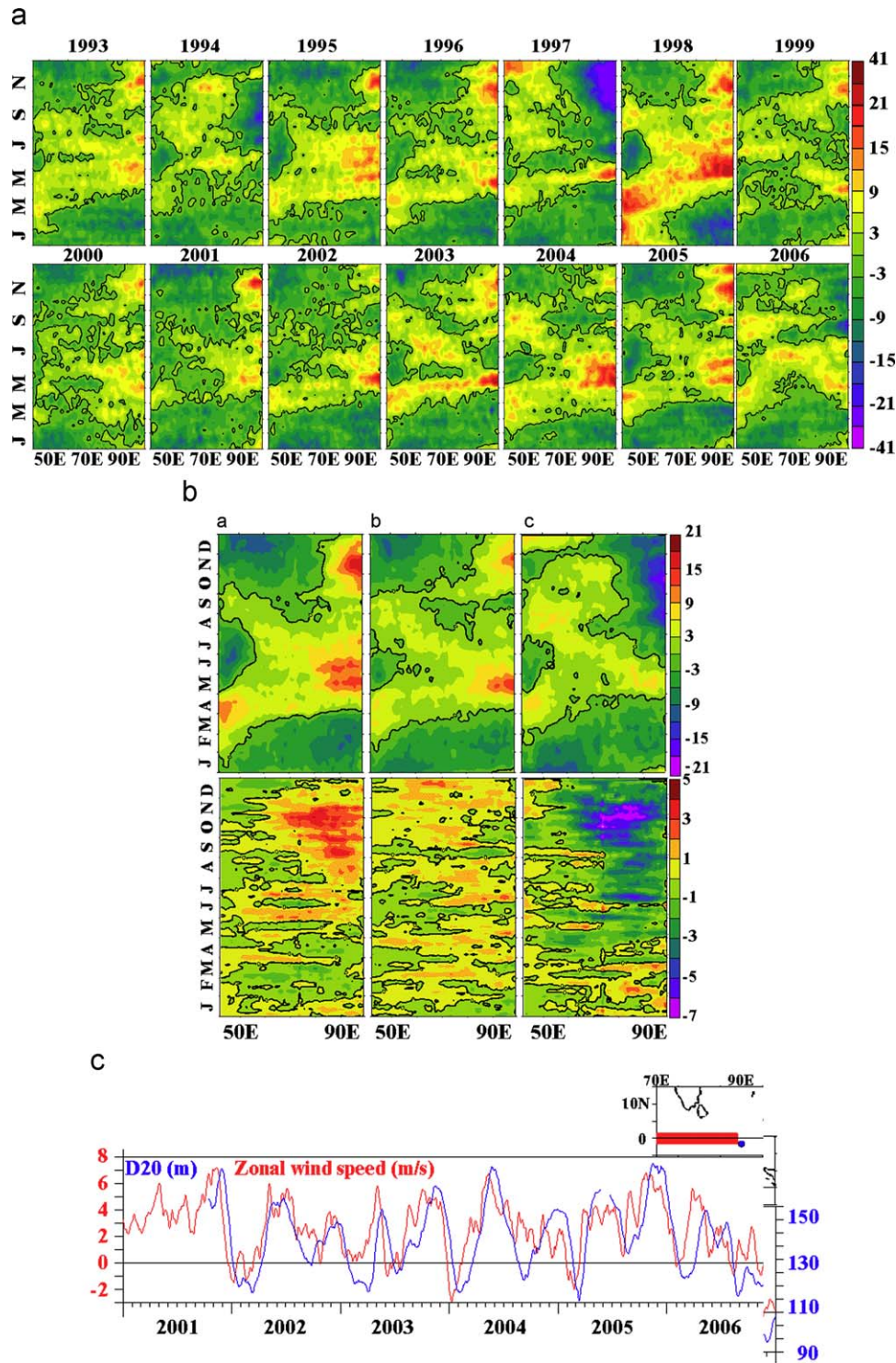


Fig. 4. (a) Longitude-time plots of the interannual variability of SSHA (cm) along the equator in the Indian Ocean during January–December for years 1993–2006. (b) Composite longitude-time plots of SSHA (cm) (top panel) and zonal wind speed anomalies (m/s) (bottom panel) along the equator in the Indian Ocean during January–December for the years when the second downwelling Kelvin wave is (a) strong (b) weak and (c) absent during the IOD years. (c) Time series of QuikSCAT surface wind speed (m/s) (averaged over the red box bounded by 70°E, 90°E, 1°N and 1°S shown in the map) and D20 (m) from JAMSTEC mooring located at 1.5°S and 90°E (blue dot shown in the map) during 2001–2006 (for interpretation of the references to color in this figure legend, the reader is referred to the web version of this article).

rotating eddy (inferred from circulation – Ekman component estimated from QuikSCAT winds and geostrophic component estimated from SSHA) spins up (Fig. 3g). The western flank of this eddy moves poleward along the east coast of India opposing the equatorward propagating first upwelling Kelvin wave. In addition, during April–May, the EICC also flows poleward along the east coast of India (Fig. 3h). Both these systems appear to block or

weaken the propagation of the first upwelling Kelvin wave in the coastal wave guide of the western BoB. The EICC appears to continue to have its influence in arresting the propagation of the first downwelling Kelvin wave (left panel of Fig. 3h). As mentioned earlier, the second upwelling Kelvin wave is least developed and is limited to the southeastern rim of the BoB. The signature of this wave along the equator is also weaker, as seen in

the SSHA and D20 anomaly fields shown in Fig. 2. On the other hand, during October–December, the EICC flowing towards the equator along the east coast of India favours the reinforcement of the equatorward propagation of the second downwelling Kelvin wave (Fig. 3h). Thus the prevailing clockwise eddy at the head of the BoB and the associated circulation along the east coast of India appear to play a key role in modulating the propagation of the Kelvin waves in the western coastal wave guide of the BoB.

3.4. Interannual variability of the Kelvin waves in the EIO

Along the equator, the observed SSHA field shows considerable interannual variability in the eastward propagation of both the upwelling and the downwelling Kelvin waves (Fig. 4a). As the second downwelling Kelvin wave only reaches the southwest coast of India, the interannual variability of this wave is of greater interest and significance for this study. The maxima in the SSHA manifested by this downwelling Kelvin wave in the eastern EIO also show large interannual variability. The SSHA in the eastern EIO averaged for October–December representing the period of second downwelling wave are stratified into ‘strong’ (> 10 cm), ‘weak’ (0–10 cm) and ‘Indian Ocean Dipole (IOD)’ (< 0 cm) regimes. During period 1993–2006, the second downwelling Kelvin wave is stronger (weaker) during years 1995, 1996, 1998, 2001 and 2005 (1993, 1999, 2000, 2002, 2003 and 2004). On the other hand the signature of this downwelling Kelvin wave is completely absent during the IOD years 1994, 1997 and 2006. The composites of the ‘strong’, the ‘weak’ and the ‘IOD’ regimes show significant differences in the signatures of the second downwelling Kelvin wave (Fig. 4b). During the IOD years, the first downwelling Kelvin wave is much weaker and the second downwelling Kelvin wave is completely absent as the upwelling signal in the eastern EIO is most pronounced (Saji et al., 1999; Webster et al., 1999; Vinayachandran et al., 2002; Rao et al., 2002; Feng and Meyers, 2003; Gnanaseelan et al., 2003; Prasad and McClean, 2004). The zonal winds along the equator also show strong intraseasonal and interannual variability that is more pronounced during boreal fall (Fig. 3f). The composites of zonal winds along the equator for all three regimes also show striking differences during boreal fall (Fig. 4b). The zonal winds are stronger along the eastern equator during the ‘strong’ regime compared with the ‘weak’ regime. These stronger winds have resulted in stronger downwelling Kelvin waves as seen in the larger positive values of SSHA in the eastern EIO during October–December. However, during the IOD regime, the equatorial westerlies are replaced by strong easterlies resulting in large negative SSHA in the eastern EIO. Thus it is clear that the observed interannual variability seen in the equatorial zonal winds distinctly shows its signature in the SSHA field through eastward propagating Kelvin waves.

Changes in thermocline depth can be directly driven by the local winds as well as by remote effects through the propagating waves in the equatorial ocean. The continuous time series measurements of near-surface thermal structure made from a mooring deployed in the eastern EIO by JAMSTEC have provided a unique data set to examine the observed interannual variability of D20 forced by the local winds and the propagating Kelvin waves (Fig. 4c). The time series of both the temporally smoothed QuikSCAT surface zonal wind speed averaged over a rectangular box in the central EIO and D20 at a station located in the eastern EIO show strong semi-annual periodicity with maxima coinciding with the monsoon transitions during the observational record of 2001–2006. In general the surface zonal wind speed and D20 are phase locked with a correlation coefficient of 0.83, when the D20 lags the surface zonal wind speed by 3 weeks in close agreement

with Hase et al. (2008). Large year-to-year variability is also seen in the surface zonal wind speed and D20 maxima during the fall transition. Clearly the surface zonal wind speed and D20 during the fall transition are higher (lower) during 2001 and 2005 (2002, 2003 and 2004) years of ‘strong’ (‘weak’) second downwelling Kelvin wave activity. However, during 2006 the observed pattern of surface zonal wind speed and D20 is anomalous because of active IOD.

3.5. Interannual variability of the Kelvin waves in the coastal wave guides of the BoB and the southeastern AS

Numerical experiments (McCreary et al., 1996; Shankar et al., 1996) have suggested that the coastal Kelvin waves can also have significant impact on the EICC in the BoB. As large interannual variability is noticed in the second downwelling Kelvin wave activity along the eastern EIO, a corresponding variability is also expected in the coastal wave guides of the BoB and the coastal southeastern AS. The observed SSHA data extracted for 129 boxes (starting from the box located on the easternmost equator) closest to the coast well within the Rossby radius of deformation in the BoB and the southeastern AS (wave track shown in Fig. 5A) are utilized to construct the wave track-time fields for the individual years. The observed annual cycle of SSHA clearly depicts the signature of the two pairs of propagating upwelling and downwelling Kelvin waves along the coastal wave guide of the BoB (Fig. 5B). The observed negative (positive) values of SSHA along the eastern and the northern rims of the BoB depict the signatures of the upwelling (downwelling) Kelvin waves during January–March and August–September (April–June and October–December) propagating counterclockwise. As seen over the equator, large interannual variability in the Kelvin wave activity is also noticed in the coastal wave guides of the BoB and the southeastern AS (Fig. 5B).

The composites of these three categories of years have also correspondingly shown significant differences in the second downwelling Kelvin wave signatures and in some measure for the first downwelling Kelvin wave during May–June (Fig. 5C). During the ‘strong’ regime the amplitude of the second downwelling Kelvin wave is greater in the coastal BoB, clearly indicating the importance of local alongshore wind stress as suggested by the modeling study of McCreary et al. (1993). But it is also interesting to note the weakening amplitude of this wave as it approaches the wave guide of the southeastern AS. During the IOD years, the first downwelling Kelvin wave is also much weaker and the second downwelling Kelvin wave is completely absent as the upwelling signal in the eastern EIO is more pronounced. As these Kelvin waves are driven by the equatorial zonal winds, it would be appropriate to examine their corresponding composites for all three regimes. The observed anomalies of the zonal wind speed for these three categories of years also show large differences during the second-half of the year over the eastern EIO (Fig. 4b). During the ‘strong’ regime, the anomalies are positive and stronger during September–November in the eastern region. During the ‘weak’ regime, the anomalies are positive but are much weaker during September–November. During the ‘IOD’ regime, the anomalies are negative and stronger from May–June onwards, peaking during October–November. Thus, it is clear that the zonal winds in the eastern EIO play a very important role in determining the strength of both the upwelling and downwelling Kelvin waves that propagate into the wave guides of the coastal BoB in accordance with Han and Webster (2002).

In general, in close agreement with the observed interannual variability in the eastern EIO, the ‘strong’ and the ‘weak’ regimes

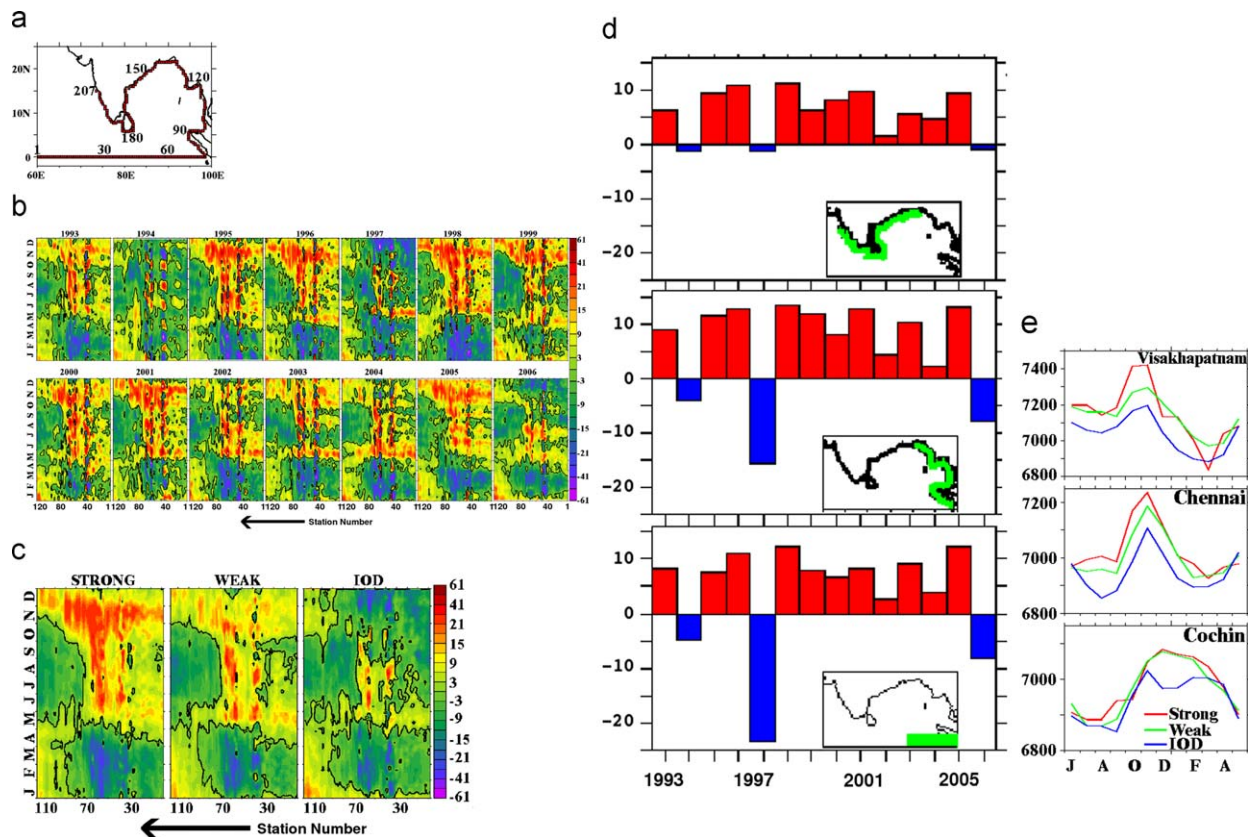


Fig. 5. (A) Distribution of one degree boxes along the coastal wave guides of the BoB and southeastern AS (station 1 starts at the eastern edge of the equator and the numbers are shown at an interval of 30) where SSHA data are utilized to track the propagation of the coastal Kelvin waves. (B) Wave track-time plots of the interannual variability of SSHA (cm) off the coasts of the BoB and southeastern AS during 1993–2006 (wave track shown in Fig. 5A). (C) Composite wave track-time plots of SSHA (cm) from the eastern equator to the southwest coast of India (wave track shown in Fig. 5A) during the years when the second downwelling Kelvin wave is (a) strong (b) weak and (c) absent during the IOD years. (D) Interannual variability of October–December averaged SSHA (cm) in the eastern equatorial region (average of the green boxes shown in the inset map of the bottom panel) and along the coastal wave guides of the BoB and the southeastern AS (average of the green boxes shown in the inset map of the upper panels). (E) Observed monthly composites of sea level data (mm) recorded by tide gauges at Visakhapatnam, Chennai, and Cochin (station locations shown in Fig. 3e) (for interpretation of the references to color in this figure legend, the reader is referred to the web version of this article).

of the second downwelling Kelvin wave are also seen during October–December in the coastal wave guides of the BoB and the southeastern AS with a very high degree of correspondence (Fig. 5D). The correlation between the SSHA in the eastern EIO and the SSHA along the eastern rim of the BoB is 0.97, and the corresponding correlation between SSHA in the eastern EIO and the SSHA along the western rim of the BoB and along the southwest coast of India is 0.84. There is also a close resemblance in the second downwelling Kelvin wave activity along the equator and along the eastern rim of the BoB during the ‘IOD’ years. However, a big reduction in the amplitude of SSHA is seen along the western rim of the BoB and along the southwest coast of India during the IOD years. The increase in the positive values during the non-IOD years along the eastern rim of the BoB is clearly consistent with the role of alongshore wind stress in the BoB (McCreary et al., 1993).

The observed sea-level data as recorded by tide gauge stations on the east coast of India (Visakhapatnam and Chennai) composited for ‘strong’, ‘weak’ and ‘IOD’ regimes during October–December also show significant differences (Fig. 5f). During September–November, the sea level is highest during the ‘strong’ regime and lowest during the ‘IOD’ regime. Interestingly, the observed differences between the ‘strong’ and the ‘weak’ regimes at a station on the southwest coast of India (Cochin) are negligible, although the observed sea level is lowest during the ‘IOD’ regime.

3.6. Interannual variability of the westward propagating Rossby waves in the northern EIO

It is well known that the poleward propagating upwelling (downwelling) Kelvin waves along the eastern rim of the BoB also trigger upwelling (downwelling) Rossby waves that propagate westward with latitude-dependent phase speed (Chelton et al., 1998). In response to the triggering of the Kelvin waves, two pairs of upwelling and downwelling Rossby waves propagate westward alternately in a year. Among the two upwelling and two downwelling Rossby waves it is shown that the second downwelling Rossby wave is the most pronounced. In the latitude band 2–6°N, the westward propagation of Rossby wave triggered by the northward propagating second downwelling wave is therefore examined in the SSHA field (Fig. 6a). The composites for all the three regimes show large differences in the amplitude of this wave. Clearly the westward propagating Rossby wave is more pronounced during the ‘strong’ regime than during the ‘weak’ regime. On the other hand, the westward propagation during the ‘IOD’ regime is not seen from the eastern rim of the BoB, as the upwelling off the Sumatra coast overwhelms the regular second downwelling Kelvin wave, as shown in Figs. 4b and 5B. Yu (2003) has also shown how the observed interannual variability of the 20 °C isotherm topography along 6°N in the BoB is most sensitive to remote interannual wind variability along the equator. Thus, it is clear that the interannual variability of the westward

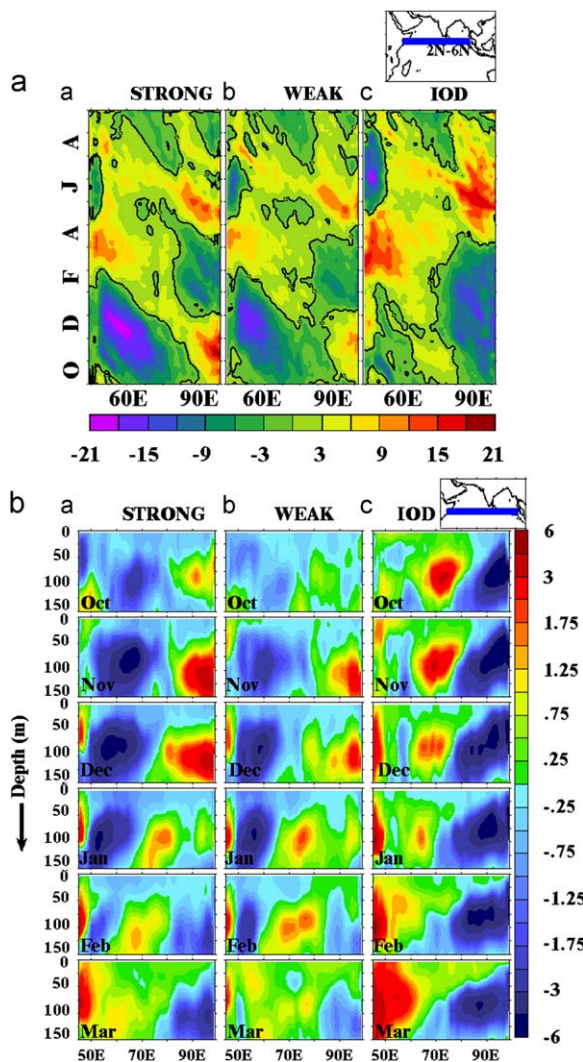


Fig. 6. (A) Composite longitude-time fields of SSHA (cm) along the latitudinal band 2°N–6°N in the north EIO (shown as blue band in the top inset map) during the following year from October when the second downwelling Kelvin wave is (a) strong (b) weak and (c) absent during the IOD years. (B) Composite of vertical thermal structure anomaly (°C) in the topmost 150 m of the water column along 2°N–6°N in the north Indian Ocean (shown as blue band in the top map) during October–March (in the following years) when the second downwelling Kelvin wave is (a) strong (b) weak and (c) absent during the IOD years (for interpretation of the references to color in this figure legend, the reader is referred to the web version of this article).

propagating Rossby wave is determined by the corresponding interannual variability of the second downwelling Kelvin wave that propagates along the equator and along the southeastern rim of the BoB, in close agreement with Yu (2003). As the signatures of the Rossby waves can be clearly seen in the subsurface thermal structure, the composites of monthly anomalies of near-surface thermal structure (annual mean removed) derived from SODA analysis (Carton et al., 2000) for the same latitude band during October–March, corresponding to all the three regimes is examined (Fig. 6b). Large differences are clearly seen among the three regimes. It is clearly evident that the positive anomaly in the thermal field and its westward propagation from the eastern boundary is more pronounced during the ‘strong’ regime compared with that of the ‘weak’ regime. However, during the ‘IOD’ regime the anomaly is negative with large amplitude in the eastern region because of intense upwelling.

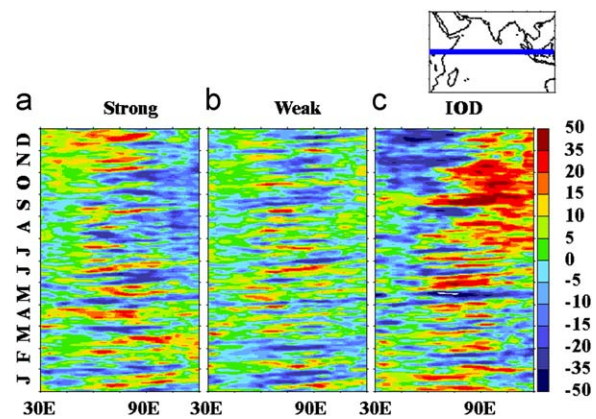


Fig. 7. Composites of longitude-time plots of OLR anomalies (W/m^2) along the equator in the Indian Ocean (shown as the blue band in the map) during January–December when the second downwelling Kelvin wave is (a) strong (b) weak and (c) absent during the IOD years (for interpretation of the references to color in this figure legend, the reader is referred to the web version of this article).

3.7. Interannual variability of equatorial westerlies in relation to moist atmospheric convection

A warm ocean surface has the potential to trigger organized moist convection under favorable meteorological conditions that generate heat in the troposphere. The zonal wind field over the EIO responds to such a heat source over the warm pool in the eastern EIO and the western equatorial Pacific Ocean. The strength of the westerlies and the magnitude of the OLR anomalies are dynamically coupled over this equatorial region (Saji et al., 1999). The composites of OLR anomalies for all the three regimes over the eastern EIO show distinct differences (Fig. 7). Over the eastern EIO, during the ‘strong’ regime the intraseasonal moist convection signals are more pronounced during July–October than they are during the ‘weak’ regime. During the ‘IOD’ regime, the east–west reversal of convection maxima during the second-half of the year is also distinctly seen in tune with the reversal of SST maxima. Thus it is clear that during the boreal fall the strength of the zonal winds over the equator driven by the east–west gradient of the heat sources in the troposphere is a critical factor in determining the observed interannual variability of the second downwelling Kelvin wave in the eastern EIO, the coastal BoB, and the southeastern AS.

4. Conclusions

The satellite-altimeter-derived SSHA fields in the tropical Indian Ocean show a distinct annual cycle in response to local Ekman pumping and the propagating waves that are remotely forced with differential importance in the spatio-temporal domain. Along the equator, during a year, two pairs of upwelling and downwelling Kelvin waves propagate alternately eastward. After hitting the Sumatra coast, they bifurcate and propagate as two coastally-trapped Kelvin waves, one northward and the other southward. The northern branches propagate over varied distances along the coastal wave guide of the BoB. In the BoB, the first upwelling (downwelling) Kelvin wave occurs during January–March (May–August) and the second upwelling (downwelling) Kelvin wave occurs during August–September (October–December). All four Kelvin waves show distinct life cycles limited to the coastal wave guide of the BoB, the only exception being the second downwelling Kelvin wave. The first upwelling Kelvin while propagating along the wave guide weakens off the western rim of the BoB and terminates off the southeast coast of India.

This suggests that this first upwelling Kelvin wave has a limited role in remotely triggering coastal upwelling observed off the southwest coast of India as early as February/March. The propagation of the first downwelling Kelvin wave also terminates mid-way in the coastal wave guide of the head of the BoB. Among the two the pairs of upwelling and downwelling Kelvin waves, the second downwelling Kelvin wave is the most pronounced. It propagates all through the coastal wave guide of the BoB, turns around Sri Lanka, and enters the southeastern AS.

The westerly winds in the equatorial region are stronger and wider in spatio-temporal extent during the boreal fall transition than during the boreal spring transition. This differential forcing partially accounts for the differences in the pathways of the first and second downwelling Kelvin waves in the coastal wave guide of the BoB. At the head of the BoB, during December–February, the western flank of a clockwise rotating eddy circulation opposes the equatorward propagating first upwelling Kelvin wave. In addition, during April–May, the EICC also flows poleward along the east coast of India. Thus both these systems appear to arrest or weaken the propagation of the first upwelling and first downwelling Kelvin waves in the coastal wave guide of the western BoB. On the other hand, the equatorward flowing EICC during October–December favours the propagation of the second downwelling Kelvin wave into the southeastern AS.

The SSHA in both the equatorial and coastal wave guides show significant differences in the signatures of the second downwelling Kelvin wave for all the three regimes, ‘strong’, ‘weak’ and ‘IOD’. The maxima in the SSHA manifested by the second downwelling Kelvin wave in the eastern EIO show large interannual variability. The zonal winds along the equator also show strong intraseasonal and interannual variability. These winds are stronger along the eastern EIO during the ‘strong’ regime than during the ‘weak’ regime. Thus, it is clear that the observed interannual variability seen in the equatorial zonal winds distinctly shows its influence on the SSHA field through eastward propagating Kelvin waves. The D20 derived from the east central EIO mooring has also shown an excellent correspondence with the surface zonal wind speed in the central EIO during the boreal fall transition on an interannual time scale suggesting the important role of the eastward propagating second downwelling Kelvin wave. As seen along the equator, large interannual variability in the Kelvin wave activity is also noticed in the coastal wave guides of the BoB and the southeastern AS. The observed anomalies of the zonal wind speed for these three categories of years also show large differences during the second-half of the year over the eastern EIO. The sea-level data recorded by tide gauge stations on the east coast of India (Visakhapatnam and Chennai), composited for all the three regimes during October–December, also show significant differences.

These Kelvin waves also trigger Rossby waves from the eastern rim of the BoB that propagate westward in the BoB and in the northern EIO. It is also clear that the interannual variability of the westward propagating Rossby wave is determined by the corresponding interannual variability of the second downwelling Kelvin wave that propagates along the equator and off the southeastern rim of the BoB. The composites of anomalies of near-surface thermal structure derived from SODA analysis for the northern EIO during October–March also show large differences for all three regimes in both the sign and the amplitude of the westward propagating Rossby wave. The composites of OLR anomalies for all three regimes over the eastern EIO also show distinct differences. During July–October, over the eastern EIO, greater moist convection is noticed during the ‘strong’ regime than during the ‘weak’ regime. During the ‘IOD’ regime, the east–west reversal of convection maxima during the second-half of the year is also distinctly seen in tune with the reversal of SST

maxima. Thus it is clear that the strength of the zonal winds over the equator driven by the east–west gradient of the tropospheric heat sources is a critical factor in determining the observed interannual variability of the second downwelling Kelvin wave in the eastern EIO and in the coastal wave guides of the BoB and the southeastern AS.

Acknowledgements

Highest appreciation is placed on record for the excellent compilation by several persons and organization of all the data sets utilized in this study. Graphics were generated using Ferret. The encouragement and the facilities provided by the Directors of NPOL, INCOIS, and NIO are gratefully appreciated. The comments from three anonymous reviewers were very helpful in improving the quality of the paper. Special thanks to the Editor for his useful editorial corrections and comments. This research is supported through INDOMOD-SATCORE Project of Ministry of Earth Sciences, Government of India.

References

- Ali, M.M., Sharma, R., Chenny, R., 1998. An atlas of the north Indian Ocean eddies from TOPEX altimeter derived sea surface heights. Indian Space Research Organization Special Publication, ISRO-SAC-SP-69-98, 8 pp., 39 plates.
- Basu, S., Meyers, S.D., O'Brien, J.J., 2000. Annual and interannual sea level variations in the Indian Ocean from TOPEX/Poseidon observations and ocean model simulations. *Journal of Geophysical Research* 105 (C1), 975–994.
- Brandt, P., Stramma, L., Schott, F., Fischer, J., Dengler, M., Quadfasel, D., 2002. Annual Rossby waves in the Arabian Sea from TOPEX/POSEIDON altimeter and in-situ data. *Deep-Sea Research II* 49, 1197–1210.
- Bruce, J.G., Johnson, D.R., Kindle, J.C., 1994. Evidence for eddy formation in the eastern Arabian Sea during the northeast monsoon. *Journal of Geophysical Research* 99 (C4), 7651–7664.
- Bruce, J.G., Kindle, J.C., Kantha, L.H., Kerling, J.L., Bailey, J.F., 1998. Recent observations and modeling in the Arabian Sea Laccadive High region. *Journal of Geophysical Research* 103 (C4), 7593–7600.
- Cane, M., 1980. On the dynamics of the equatorial currents, with application to the Indian Ocean. *Deep-Sea Research* 27A, 525–544.
- Carton, J., Chepurin, G., Cao, X., Giese, B., 2000. A simple ocean data assimilation analysis of the global upper ocean 1950–95. Part-I. Method. *Journal of Physical Oceanography* 30, 294–309.
- Chambers, D.P., Tapley, B.D., Stewart, R.H., 1999. Anomalous warming in the Indian Ocean coincident with El Niño. *Journal of Geophysical Research* 104, 3035–3047.
- Chelton, D.B., Deszoeke, R.A., Schlax, M.G., 1998. Geographic variability of the first baroclinic Rossby wave deformation. *Journal of Physical Oceanography* 28, 433–460.
- Clark, A.J., Liu, X., 1993. Observations and dynamics of semiannual and annual sea levels near the eastern equatorial Indian Ocean boundary. *Journal of Physical Oceanography* 23 (2), 386–399.
- Clark, A.J., Liu, X., 1994. Interannual sea level northern and eastern Indian Ocean. *Journal of Physical Oceanography* 24 (6), 1224–1235.
- Cutler, A.N., Swallow, J.C., 1984. Surface currents of the Indian Ocean (to 25N, 100E): compiled from historic data archived by the Meteorological Office, Bracknell, UK, Institute of Ocean Science. Report No. 187, 8 pp., 36 charts.
- Duing, W., 1970. The Monsoon Regime of the Currents in the Indian Ocean, International Indian Ocean Expedition Oceanographic Monographs Number 1. East–West Center Press, Honolulu 68 pp.
- Eigenheer, A., Quadfasel, D., 2000. Seasonal variability of the BoB circulation inferred from TOPEX/Poseidon altimetry. *Journal of Geophysical Research* 105 (C2), 3243–3252.
- Feng, M., Meyers, G., 2003. Interannual variability in the tropical Indian Ocean: a two year time scale of Indian Ocean Dipole. *Deep-Sea Research II* 50, 2263–2284.
- Fu, L.L., 2001. Ocean circulation and variability from satellite altimetry. In: Siedler, G., Church, J., Gould, J. (Eds.), *Ocean Circulation and Climate, Observing and Modelling the Global Ocean*, International Geophysics Series Number, vol. 77, pp. 141–172, plates 3.1.4–3.4.5 (Chapter 3).
- Gent, P., O'Neill, K., Cane, M., 1983. A model of the semi-annual oscillation in the equatorial Indian Ocean. *Journal of Physical Oceanography* 13, 2148–2160.
- Gnanaseelan, C., Chowdary, J.S., Misra, A.K., Salvekar, P.S., 2003. Indian Ocean dipole mode events in a simple mixed layer ocean model. *Indian Journal of Marine Sciences* 32 (4), 294–304.
- Gopalakrishna, V.V., Rao, R.R., Nisha, K., Girishkumar, M.S., Pankajakshan, T., Ravichandran, M., Johnson, Z., Girish, K., Aneeshkumar, N., Srinath, M., Rajesh, S., Rajan, C.K., 2008. Observed anomalous upwelling in the Lakshadweep Sea

- during the summer monsoon season of 2005. *Journal of Geophysical Research* 113, C05001, doi:10.1029/2007/JC004240.
- Gopalan, A.K.S., Gopalakrishna, V.V., Ali, M.M., Sharma, R., 2000. Detection of BoB eddies from TOPEX and sea truth observations. *Journal of Marine Research* 58, 721–734.
- Han, W., 2005. Origins and dynamics of the 90-day and 30–60 day variations in the equatorial Indian Ocean. *Journal of Physical Oceanography* 35, 708–728.
- Han, W., McCreary, J.P., Anderson, D.L.T., Mariano, A.J., 1999. On the dynamics of the eastward surface jets in the equatorial Indian Ocean. *Journal of Physical Oceanography* 29, 2191–2209.
- Han, W., Lawrance, D.M., Webster, P.J., 2001. Dynamical response of equatorial Indian Ocean to intraseasonal winds: zonal flow. *Geophysical Research Letters* 28 (22), 4215–4218.
- Han, W., Webster, P.J., 2002. Forcing mechanisms of sea level interannual variability in the BoB. *Journal of Physical Oceanography* 32 (1), 216–239.
- Hareesh Kumar, P.V., Sanilkumar, K.V., 2004. Long period waves in the coastal regions of north Indian Ocean. *Indian Journal of Marine Science* 33 (2), 150–154.
- Hase, H., Masumoto, Y., Kuroda, Y., Mizuno, K., 2008. Semiannual variability in temperature and salinity observed by Triangle Trans-Ocean Buoy Network (TRITON) buoys in eastern tropical Indian Ocean. *Journal of Geophysical Research* 113, C01016, doi:10.1029/2006/JC004026.
- Hastenrath, S., Greischar, L., 1991. The monsoonal current regimes of the tropical Indian Ocean: observed surface flow fields and their geostrophic and wind components. *Journal of Geophysical Research* 96 (C7), 12,619–12,633.
- Haugen, V.E., Johannessen, O.M., Evensen, G., 2002. Indian Ocean: validation of the Miami Isopycnic Coordinate Ocean Model and ENSO events during 1958–1998. *Journal of Geophysical Research* 107 (C5), 3043, doi:10.1029/2000/JC000330.
- Horii, T., Hase, H., Ueki, I., Masumoto, Y., 2008. Oceanic precondition and evolution of the 2006 Indian Ocean Dipole. *Geophysical Research Letters* 35, L03607, doi:10.1029/2007GL032464.
- Iskandar, I., Masumoto, Y., Mizuno, K., 2009. Subsurface equatorial zonal current in the eastern Indian Ocean. *Journal of Geophysical Research* 114, C06005, doi:10.1029/2008/JC005118.
- Jensen, T.G., 1993. Equatorial variability and resonance in a wind driven Indian Ocean model. *Journal of Geophysical Research* 98 (C12), 22533–22552.
- Kindle, J.C., Thompson, J.D., 1989. The 26–50 days oscillation in the western Indian Ocean: model results. *Journal of Geophysical Research* 94, 4721–4736.
- Le Blanc, J.L., Boulanger, J.P., 2001. Propagation and reflection of long equatorial waves in the Indian Ocean from TOPEX/Poseidon data during the 1993–1998 period. *Climate Dynamics* 17, 547–557.
- Lighthill, M.J., 1969. Dynamic response of the Indian Ocean to the onset of the southwest monsoon. *Philosophical Transactions of the Royal Meteorological Society A* 265, 45–92.
- Locarnini, R.A., Mishonov, A.V., Antonov, J.I., Boyer, T.P., Garcia, H.E., 2006. *World Ocean Atlas 2005, vol. 1: temperature*. In: Levitus, S. (Ed.), NOAA Atlas NESDIS 61. US Government Printing Office, Washington, DC, pp. 182.
- Luther, M.E., O'Brien, J.J., 1985. A model of the seasonal circulation in the Arabian Sea forced by observed winds. *Progress in Oceanography* 14, 353–385.
- Masumoto, Y., Meyers, G., 1998. Forced Rossby waves in the southern tropical Indian Ocean. *Journal of Geophysical Research* 103 (C12), 27,589–27,602.
- Masumoto, Y., Hase, H., Kuroda, Y., Matsuura, H., Takeuchi, K., 2005. Intraseasonal variability in the upper layer currents observed in the eastern equatorial Indian Ocean. *Geophysical Research Letters* 32, L02607, doi:10.1029/2004GL021896.
- Masumoto, Y., Horii, T., Ueki, I., Hase, H., Ando, K., Mizuno, K., 2008. Short-term upper ocean variability in the central equatorial Indian Ocean during 2006 Indian Ocean Dipole event. *Geophysical Research Letters* 35, L14S09, doi:10.1029/2008GL038334.
- McCreary, J.P., Kundu, P.K., Molinari, R.L., 1993. A numerical investigation of dynamics, thermodynamics and the mixed layer processes in the Indian Ocean. *Progress in Oceanography* 31, 181–244.
- McCreary, J.P., Han, W., Shankar, D., Shetye, S.R., 1996. Dynamics of the East India Coastal Current. 2. Numerical solutions. *Journal of Geophysical Research* 101, 13993–14010.
- McPhaden, M., 1982. Variability in the central Indian Ocean. Part I: ocean dynamics. *Journal of Marine Research* 40, 157–176.
- Miyama, T., McCreary, J.P., Sengupta, D., Senan, R., 2006. Dynamics of biweekly oscillations in the equatorial Indian Ocean. *Journal of Physical Oceanography* 36 (5), 827–846.
- Molinari, R., Olson, D., Reverdin, G., 1990. Surface current distributions in the tropical Indian Ocean derived from compilations of surface buoy trajectories. *Journal of Geophysical Research* 95 (C5), 7217–7238.
- Moore, D.W., McCreary, J.P., 1990. Excitation of intermediate frequency equatorial waves at a western ocean boundary: with application to observations from the western Indian Ocean. *Journal of Geophysical Research* 95 (C4), 5219–5231.
- Murtugudde, R., Busalacchi, A.J., 1999. Interannual variability of the dynamics and thermodynamics of the Indian Ocean. *Journal of Climate* 12, 2300–2326.
- Murtugudde, R., McCreary, J.P., Busalacchi, A.J., 2000. Oceanic processes associated with anomalous events in the Indian Ocean with relevance to 1997–1998. *Journal of Geophysical Research* 105, 3295–3306.
- Nagura, M., McPhaden, M.J., 2008. The dynamics of zonal current variations in the central equatorial Indian Ocean. *Geophysical Research Letters* 35, L23603, doi:10.1029/2008GL035961.
- O'Brien, J.J., Hurlburt, H.E., 1974. An equatorial jet in the Indian Ocean: theory. *Science* 184, 1075–1077.
- Ogata, T., Sasaki, H., Murty, V.S.N., Sarma, M.S.S., Masumoto Y., 2008. Intraseasonal meridional current variability in the eastern equatorial Indian Ocean. *J. Geophys. Res.*, 113, C07037, doi:10.1029/2007/JC004331.
- Perigaud, C., Delecluse, P., 1992. Annual sea level variations in the southern tropical Indian Ocean from Geosat and shallow-water simulations. *Journal of Geophysical Research* 97 (C12), 20,169–20,178.
- Perigaud, C., Delecluse, P., 1993. Interannual sea level variations in the tropical Indian Ocean from Geosat and shallow-water simulations. *Journal of Physical Oceanography* 23 (9), 1916–1934.
- Peter, B.N., Mizuno, K., 2000. Annual cycle of steric height in the Indian Ocean estimated from thermal field. *Deep-Sea Research I* 47, 1351–1368.
- Polito, P.S., Liu, W.T., 2003. Global characterization of Rossby waves at several spectral bands. *Journal of Geophysical Research* 108 (C1), 3018, doi:10.1029/2000JC000607.
- Potemra, J.T., Luther, M.E., O'Brien, J.J., 1991. The seasonal circulation of the upper ocean in the BoB. *Journal of Geophysical Research* 96 (12), 12,667–12,683.
- Prasad, T.G., Ikeda, M., 2001. Spring evolution of Arabian Sea High in the Indian Ocean. *Journal of Geophysical Research* 106 (C11), 31,085–31,098.
- Prasad, T.G., McClean, J.L., 2004. Mechanisms of anomalous warming in the western Indian Ocean during dipole mode events. *Journal of Geophysical Research* 109, C02019, doi:10.1029/2003JC001872.
- Prasannakumar, S.P., Unnikrishnan, A.S., 1995. Seasonal cycle of temperature and associated wave phenomena in the upper layers of the BoB. *Journal of Geophysical Research* 100, 13,585–13,593.
- Rahul, P.C.R., Salvekar, P.S., Deo, A.A., Ganer, D.W., 2004. Westward propagating twin gyres in the equatorial Indian Ocean. *Geophysical Research Letters* 31, L01304, doi:10.1029/2003GL018615.
- Rao, A.S., Behera, S.K., Masumoto, Y., Yamagata, T., 2002. Interannual subsurface variability in the tropical Indian Ocean with a special emphasis on the Indian Ocean Dipole. *Deep-Sea Research II* 49, 1549–1572.
- Rao, R.R., Sivakumar, R., 2000. Seasonal variability of near-surface thermal structure and heat budget of the mixed layer of the tropical Indian Ocean from a new global ocean temperature climatology. *Journal of Geophysical Research* 105 (C1), 995–1015.
- Reverdin, G., 1987. The upper equatorial Indian Ocean: the multi-year averaged seasonal cycle. *Journal of Physical Oceanography* 17, 903–927.
- Reverdin, G., Luyten, J., 1986. Near-surface meanders in the equatorial Indian Ocean. *Journal of Physical Oceanography* 16, 1088–1100.
- Saji, N.H., Goswami, B.N., Vinayachandran, P.N., Yamagata, T., 1999. A dipole mode in the tropical Indian Ocean. *Nature* 401, 360–363.
- Schiller, A., Godfrey, S., McIntosh, P.C., Meyers, G., Wijffels, S.E., 1998. Seasonal near-surface dynamics and thermodynamics of the Indian Ocean and Indonesian throughflow in a global general circulation model. *Journal of Physical Oceanography* 28, 2288–2312.
- Schott, F.A., McCreary, J.P., 2001. The monsoon circulation of the Indian Ocean. *Progress in Oceanography* 51, 1–123.
- Schott, F.A., Xie, S.P., McCreary, J.P., 2009. Indian Ocean circulation and climate variability. *Reviews of Geophysics* 47, RG1002, doi:10.1029/2007RG000245.
- Sengupta, D., Senan, R., Goswami, B.N., 2001. Origin of intraseasonal variability of circulation in the tropical central Indian Ocean. *Geophysical Research Letters* 28 (7), 1267–1270.
- Sengupta, D., Senan, R., Murty, V.S.N., Fernando, V., 2004. A biweekly mode in the equatorial Indian Ocean. *Journal of Geophysical Research* 109, C10003, doi:10.1029/2004JC002329.
- Senan, R., Sengupta, D., Goswami, B.N., 2003. Intraseasonal 'Monsoon Jets' in the equatorial Indian Ocean. *Geophysical Research Letters* 30 (14), 1750, doi:10.1029/2003GL017853.
- Shankar, D., McCreary, J.P., Han, W., Shetye, S.R., 1996. Dynamics of the East India Coastal Current. 1. Analytical solutions forced by interior Ekman pumping and local alongshore winds. *Journal of Geophysical Research* 101, 13975–13991.
- Shankar, D., Shetye, S.R., 1997. On the dynamics of the Lakshadweep high and low in the southeastern Arabian Sea. *Journal of Geophysical Research* 102 (C6), 12,551–12,562.
- Shankar, D., Vinayachandran, P.N., Unnikrishnan, A.S., 2002. The monsoon currents in the north Indian Ocean. *Progress in Oceanography* 52, 63–120.
- Shenoi, S.S.C., Saji, P.K., Almeida, A.M., 1999. Near-surface circulation and kinetic energy in the tropical Indian Ocean derived from Lagrangian drifters. *Journal of Marine Research* 57, 885–907.
- Shetye, S.R., Gouveia, A.D., 1998. Coastal circulation in the north Indian Ocean. In: Robinson, A.R., Brink, K.H. (Eds.), *The Sea*, vol. 11. John Wiley & Sons, Inc., New York, pp. 523–556.
- Somayajulu, Y.K., Murty, V.S.N., Sarma, Y.V.B., 2003. Seasonal and inter-annual variability of surface circulation in the Bay of Bengal from TOPEX/Poseidon altimetry. *Deep-Sea Research II* 50, 867–880.
- Sprintall, J., Gordon, A., Murtugudde, R., Susanto, D., 2000. A semi-annual Indian Ocean forced Kelvin wave observed in the Indonesian Seas in May 1997. *Journal of Geophysical Research* 105, 17217–17230.
- Subrahmanyam, B., Robinson, I.S., 2000. Sea surface height variability in the Indian Ocean from TOPEX /POSEIDON altimetry and model simulations. *Marine Geodesy* 23, 167–195.
- Subrahmanyam, B., Robinson, I.S., Blundell, J.R., Challenor, P.G., 2001. Indian Ocean Rossby waves observed in TOPEX/POSEIDON altimeter data and in model simulations. *International Journal of Remote Sensing* 22 (1), 141–167.

- Tsai, P.T.H., O'Brien, J.J., Luther, M.E., 1992. The 26-day oscillation in the satellite sea surface temperature measurements in the equatorial western Indian Ocean. *Journal of Geophysical Research* 97 (C6), 9605–9618.
- Vinayachandran, P.N., Shetye, S.R., Sengupta, D., Gadgil, S., 1996. Forcing mechanisms of the BoB circulation. *Current Science* 71 (10), 753–763.
- Vinayachandran, P.N., Yamagata, T., 1998. Monsoon response of the sea around Sri Lanka: generation of thermal domes and anticyclonic vortices. *Journal of Physical Oceanography* 28 (10), 1946–1960.
- Vinayachandran, P.N., Iizuka, S., Yamagata, T., 2002. Indian Ocean dipole mode events in an ocean general circulation model. *Deep-Sea Research II* 49, 1573–1596.
- Visbeck, M., Schott, F., 1992. Analysis of seasonal current variations in the western equatorial Indian Ocean: direct measurements and GFDL model comparison. *Journal of Physical Oceanography* 22 (10), 1112–1128.
- Wang, L., Koblinsky, C.J., Howden, S., 2001. Annual Rossby wave in the southern Indian Ocean: why does it 'appear' to break down in the middle ocean. *Journal of Physical Oceanography* 31 (1), 54–74.
- Webster, P.J., Moore, A.M., Loschnigg, J.P., Leben, R.R., 1999. Coupled ocean–atmosphere dynamics in the Indian Ocean during 1997–98. *Nature* 401, 356–360.
- Wentz, F.J., Gentemann, C., Smith, D., Chelton, D., 2000. Satellite measurements of sea surface temperature through clouds. *Science* 288, 847–850.
- Wentz, F.J., Smith, D.K., Mears, C.A., Gentemann, C.L., 2001. In: *Advanced Algorithms for QuikSCAT and SeaWinds/AMSR Geoscience and Remote Sensing Symposium, IGARSS*, vol. 3, IEEE 2001 International, pp. 1079–1081.
- White, W., 2000. Coupled Rossby waves in the Indian Ocean on interannual time scales. *Journal of Physical Oceanography* 30 (11), 2972–2988.
- Woodbury, K.E., Luther, M.E., O'Brien, J.J., 1989. The wind driven seasonal circulation in the southern tropical Indian Ocean. *Journal of Geophysical Research* 94, 17,985–18,002.
- Wyrtki, K., 1971. *Oceanographic Atlas of the International Indian Ocean Expedition*. National Science Foundation, Washington, DC 531 pp.
- Wyrtki, K., 1973. An equatorial jet in the Indian Ocean. *Science* 181, 262–264.
- Yamagata, T., Mizuno, K., Masumoto, Y., 1996. Seasonal variations in the equatorial Indian Ocean with their impacts on the Lombok Throughflow. *Journal of Geophysical Research* 101, 12465–12473.
- Yu, L., O'Brien, J.J., Yang, J., 1991. On the remote forcing of the circulation in the BoB. *Journal of Geophysical Research* 96 (C11), 20,449–20,454.
- Yu, L., 2003. Variability of the depth of the 20 °C isotherm along 6°N in the BoB: its response to remote and local forcing and its relation to satellite SSH variability. *Deep-Sea Research II* 50, 2285–2304.
- Yuan, D., Han, W., 2006. Roles of equatorial waves and western boundary reflection in the seasonal circulation of the equatorial Indian Ocean. *Journal of Physical Oceanography* 36 (5), 930–944.